Forensic Science, Medicine and Pathology
https://doi.org/10.1007/s12024-026-01274-x

ORIGINAL ARTICLE

Histological artifacts induced by the contrast agent in multi-phase post-mortem CT angiography (MPMCTA): Part II – Pathological tissues

Jessika Camatti[1] · Bruno Giuliano Gangi[2] · Maria Paola Bonasoni[3] · Giovanni Battinelli[4] · Luca Alemanno[4] · Giovanni Pizzuti[4] · Pietro Torricelli[5] · Enrico Silingardi[5] · Rossana Cecchi[5] · Anna Laura Santunione[5]

Received: 22 March 2026 / Accepted: 17 May 2026

Abstract

Multi-phase postmortem computed tomography angiography (MPMCTA) is increasingly used in forensic pathology; however, contrast medium injection may induce histo-morphological artifacts. While these artifacts have been previously described in normal tissues, their behavior in pathological conditions remains incompletely characterized. A retrospective study was conducted on 37 cases of sudden death undergoing MPMCTA. A total of 190 histological samples showing pathological alterations, previously excluded from the analysis of normal tissues, were examined. Tissue sections were processed using standard histological techniques and analyzed by experienced forensic pathologists to identify and characterize contrast-related artifacts in the presence of underlying disease. The main categories of artifacts—optically empty spaces (OES), vascular dilatation, hyperemia, and compression of adjacent structures—were consistently observed in pathological tissues. However, their distribution and morphology were frequently modified by the underlying disease. Inflammatory, neoplastic, hemorrhagic, and degenerative conditions were associated with heterogeneous contrast distribution and uneven perfusion patterns. OES were observed both within vascular lumina and in extravascular compartments, particularly in hemorrhagic and necrotic areas. Despite these alterations, the recognition of the underlying pathological processes was generally preserved. Relevant diagnostic pitfalls were identified, particularly in the differential diagnosis with fat embolism, gas-related changes, and cholesterol clefts. MPMCTA induces reproducible histo-morphological artifacts also in pathological tissues, although their distribution and appearance are influenced by the underlying disease. Awareness of these changes is essential to avoid misinterpretation. When properly recognized, contrast-related artifacts do not preclude accurate histopathological diagnosis and support the integrated use of imaging, autopsy, and histology in forensic practice.

Key points

- Multi-Phase Post-Mortem CT Angiography (MPMCTA) induces reproducible histological artifacts also in pathological tissues.
- The morphology and distribution of contrast-related artifacts may be modified by the underlying pathological process.
- Optically empty spaces (OES), vascular dilatation, hyperemia, and compression artifacts may mimic pathological findings in forensic histopathology.
- Recognition of the interaction between pathological alterations and contrast-related artifacts is essential to avoid diagnostic misinterpretation.
- Despite the presence of artifacts, the underlying pathological architecture generally remains identifiable.

Keywords Post-mortem angiography · Multi-Phase Post-Mortem Computed Tomography Angiography · Forensic imaging · Post-mortem imaging · Histological changes · Histological artifacts

Extended author information available on the last page of the article

Published online: 27 May 2026

Introduction

Postmortem imaging, particularly postmortem computed tomography (PMCT) and multiphase postmortem computed tomography angiography (MPMCTA), has become an increasingly important tool in modern forensic pathology [1, 2]. These techniques enable a detailed, non-invasive evaluation of the entire body and are widely used in the investigation of both natural and traumatic deaths. In particular, MPMCTA allows enhanced visualization of the cardiovascular system through the injection of a contrast agent using a pressure-controlled device (Virtangio®), facilitating the detection of vascular lesions such as hemorrhages, stenosis, aneurysms, and dissections [3–7].

However, the injection of contrast media is known to induce histo-morphological changes that may affect subsequent microscopic examination [6, 8, 9]. In our previous study, these changes were systematically described in normal tissues and categorized into four main groups: optically empty spaces (OES), vascular dilatation, hyperemia, and compression of adjacent structures [10]. These findings highlighted the importance of recognizing contrast-related artifacts in order to avoid potential diagnostic misinterpretation in forensic histopathology.

Despite this, a substantial proportion of histological specimens in routine forensic practice show underlying pathological alterations. The interaction between contrast media and pathological tissues remains incompletely characterized, particularly with regard to the distribution of artifacts, their morphological variability, and their potential to mimic true pathological findings. Pre-existing disease processes may alter tissue architecture, vascular integrity, and permeability, thereby influencing the behavior of the contrast agent and potentially modifying the appearance of histological artifacts.

A better understanding of these interactions is essential, as contrast-related artifacts may complicate the interpretation of pathological findings and introduce relevant diagnostic pitfalls, particularly in the differential diagnosis with fat embolism, gas-related changes, cholesterol clefts, and inflammatory vascular conditions.

Unlike normal tissues, pathological tissues may exhibit altered vascular permeability, disrupted tissue architecture, hemorrhagic infiltration, necrosis, or inflammatory vascular damage. In general, conditions associated with altered vascularization or tissue integrity may potentially modify the distribution and retention of contrast medium following MPMCTA, thereby indirectly influencing the morphology and localization of histological artifacts.

In this context, the interaction between pathological alterations and contrast-related artifacts may generate heterogeneous histological patterns and additional diagnostic pitfalls during forensic histopathological evaluation. Therefore, the present study aimed to evaluate whether the principal categories of artifacts previously described in normal tissues are similarly observed in pathological conditions, how their distribution may be modified by the underlying disease process, and whether these changes may compromise the recognition and histopathological interpretation of the underlying pathology.

Materials and methods

Casuistry

A retrospective study was performed on a cohort of 37 sudden death cases that underwent MPMCTA at the Institute of Legal Medicine of Modena, Italy, between April 2016 and July 2019. Inclusion criteria comprised cases of sudden death occurring in the Modena district in non-hospitalized individuals, in whom the cause of death could not be reliably presumed based on medical history, circumstantial information, or external examination, and in whom a natural cause of death was suspected. Cases showing advanced signs of putrefaction were excluded because of the known risk of post-mortem imaging and histological artifacts. The time interval between death and MPMCTA ranged from 10 to 99 h, with a mean of 42.2 ± 23.0 h. Based on autopsy, histological, and toxicological findings, six main categories of cause of death were identified: acute heart failure ($n = 16$); arrhythmic-based functional cardiac arrest ($n = 8$); acute myocardial infarction ($n = 5$); cardiac tamponade due to hemopericardium secondary to aortic rupture or dissection ($n = 5$); death related to neoplastic disease ($n = 2$); and pulmonary thromboembolism ($n = 1$).

A total of 494 histological samples obtained from different organs and tissues within this cohort were initially reviewed. Inclusion criteria of the present study consisted of the presence of histologically identifiable pathological alterations and adequate tissue preservation allowing reliable microscopic evaluation of MPMCTA-related artifacts. Exclusion criteria consisted of samples showing normal tissues ($n = 270$), severe autolysis ($n = 18$), insufficient organ perfusion ($n = 13$), or inadequate histological staining ($n = 3$). The remaining 190 pathological histological samples constituted the study cohort of the present investigation. These specimens were subsequently evaluated in order to investigate the morphology, localization, and distribution of MPMCTA-related histological artifacts in pathological tissues.

Protocol

All cases underwent MPMCTA according to the same standardized protocol previously adopted in Part I [10] and established by the Technical Working Group of Post Mortem Angiography Methods (TWGPAM; technical specifications available at: https://www.twgpam.org/) [11]. The imaging protocol comprised two native (unenhanced) scans followed by three contrast-enhanced angiographic phases.

The examinations were conducted using a 64-detector CT scanner (LightSpeed VCT 64, GE Healthcare, Milwaukee, WI, USA) in conjunction with the Virtangio® device to infuse a contrast agent mixture of Angiofil® (Fumedica AG, Switzerland) and paraffin oil. The slice thickness was 1.25 mm, with 0.75 mm collimation and a 512 × 512 matrix. All image reconstructions were performed on non-enhanced CT with a slice thickness of 2.0 mm, incremented by 1 mm, using soft tissue and bone kernels. The enhanced phases were reconstructed with a slice thickness of 1.0 mm, incremented by 0.5 mm, using the soft-tissue kernel.

Following radiological analysis, all bodies underwent external examination and autopsy according to the ECLFM recommendations [12]. Tissue sampling for histopathological evaluation was subsequently performed during autopsy. Specimens were collected, formalin-fixed, paraffin-embedded, sectioned, and stained with hematoxylin-eosin (H&E).

Histo-morphological analysis

The slides were examined using a semi-motorized Olympus BX53 microscope equipped with an Olympus DP21 camera for image acquisition.

The analysis was performed in consecutive reading sessions by three forensic pathologists with more than 20 years of experience in histopathology. Microscopic findings were reviewed during consecutive evaluation sessions, and cases showing interpretative uncertainty were jointly re-evaluated until consensus was achieved. Histological assessment was not performed under formal blinded conditions, since radiological-pathological correlation represented an integral component of the forensic interpretative workflow adopted in the present study.

For the purpose of the present study, MPMCTA-related histological artifacts were classified according to their predominant morphological appearance into four principal categories: 1. OES: (a) Intravascular OES: empty spaces located within vascular lumina, frequently associated with dark granular residues; (b) Extravascular OES: empty spaces identified outside vascular structures, typically within hemorrhagic, necrotic, or structurally disrupted tissues; 2. Vascular dilatation: artificial enlargement or distension of vascular structures related to contrast medium distribution; 3. Vascular hyperemia: diffuse vascular congestion and increased intravascular accumulation of contrast-related material; 4. Compression artifacts: distortion or compression of adjacent parenchymal structures secondary to vascular distension or contrast accumulation. Artifacts were evaluated according to their morphology, localization, relationship with surrounding pathological tissues, and potential differential diagnostic implications.

Results

A total of 190 histological samples showing pathological alterations were analyzed. These specimens corresponded to the pathological samples previously excluded from the analysis of normal tissues in Part I [10] because of the presence of underlying pathological alterations.

The observed pathological conditions included inflammatory processes, neoplastic lesions, hemorrhagic infiltrations, degenerative changes, and vascular diseases. In addition to these underlying pathological findings, several histo-morphological artifacts related to contrast medium injection were identified.

As previously described in normal tissues, the artifacts mainly consisted of OES, vascular dilatation, vascular hyperemia, and compression of adjacent structures. However, the presence of pathological alterations frequently modified the distribution and morphology of these artifacts.

Central nervous system and adjacent cranial tissues

The pathological findings identified in the central nervous system included cortical atrophy, cerebral meningioma, perivascular lymphocytic infiltration, subarachnoid hemorrhage, galeal hemorrhage, and a galeal osteoma.

Cortical atrophy in cerebellar samples was characterized by corpora amylacea, which were distinguishable from OES (contrast-related artifacts) because of their extravascular localization (Fig. 1a).

Cerebral meningioma specimens showed typical neoplastic features such as whorls of meningothelial cells and psammoma bodies. Contrast-related artifacts, including intravascular OES and vascular dilatation, were found (Fig. 1b and c).

In cortical samples, *perivascular lymphocytic infiltration* was observed in association with vascular dilatation (Fig. 1d). This pattern may partially mimic vasculitic changes; however, the absence of vessel wall necrosis, fibrinoid degeneration, or structural vascular damage supported the interpretation of vascular dilatation as a contrast-related artifact rather than true vasculitis.

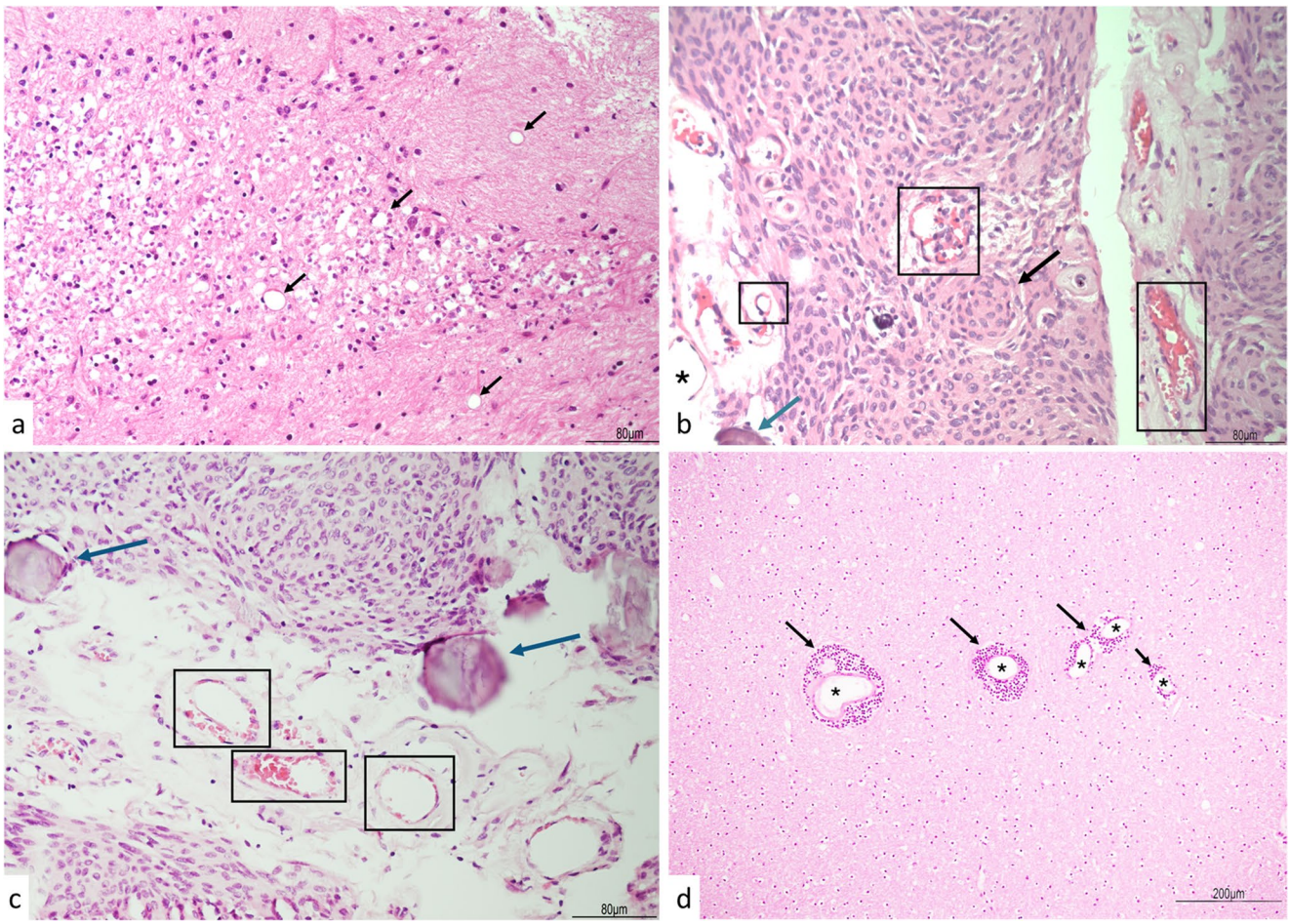

Fig. 1 Central nervous system. (**a**) Cerebellum, cortical atrophy (20×): Cortical atrophy with numerous corpora amylacea (black arrows), characterized by round to ovoid structures within the neuropil. (**b**–**c**) Cerebral meningioma (20×): Preserved neoplastic architecture with typical whorls of meningothelial cells (black arrows) and psammoma bodies (blue arrows). Intravascular OES (black boxes) and vascular dilatation (black asterisks) are present. (**d**) Cerebral cortex (10×): Perivascular lymphocytic infiltration (black arrows) associated with vascular dilatation (black asterisks)

In *subarachnoid hemorrhage* and in *galeal hemorrhage* specimens, OES were identified within hemorrhagic infiltrates (Fig. 2a and b).

In *galeal hemorrhage* samples, the differential diagnosis between OES and putrefaction-related gas bubbles was corroborated by the preservation of skin structures without post-mortem changes (Fig. 2b).

In specimens including galea and periosteum, the presence of dark granular material attributable to contrast medium residues further supported the differential diagnosis between OES and putrefaction-related gas bubbles.

(Fig. 2c).

In a *galeal osteoma*, intravascular OES were observed in association with bone and adipose tissue. Adipocytes were distinguishable from OES because of their extravascular localization and well-defined cytoplasmic membranes (Fig. 2d).

Cardiopulmonary system

The pathological processes identified in the cardiopulmonary system included myocarditis, coronary artery dissection, fibro-lipidic atherosclerotic plaques, and chronic sclerosing interstitial lung disease (UIP pattern), as well as mediastinal hemorrhage.

In *myocarditis* samples, lymphocytic infiltration surrounding myocardial fibers was observed. OES were present intravascularly, occasionally causing compression of myocardial fibers (Fig. 3a).

In cases of *coronary artery dissection*, OES associated with dark granular residues were present within the periluminal hemorrhagic infiltration (Fig. 3b).

Fibro-lipidic atherosclerotic plaques showed numerous empty spaces corresponding to cholesterol clefts. These

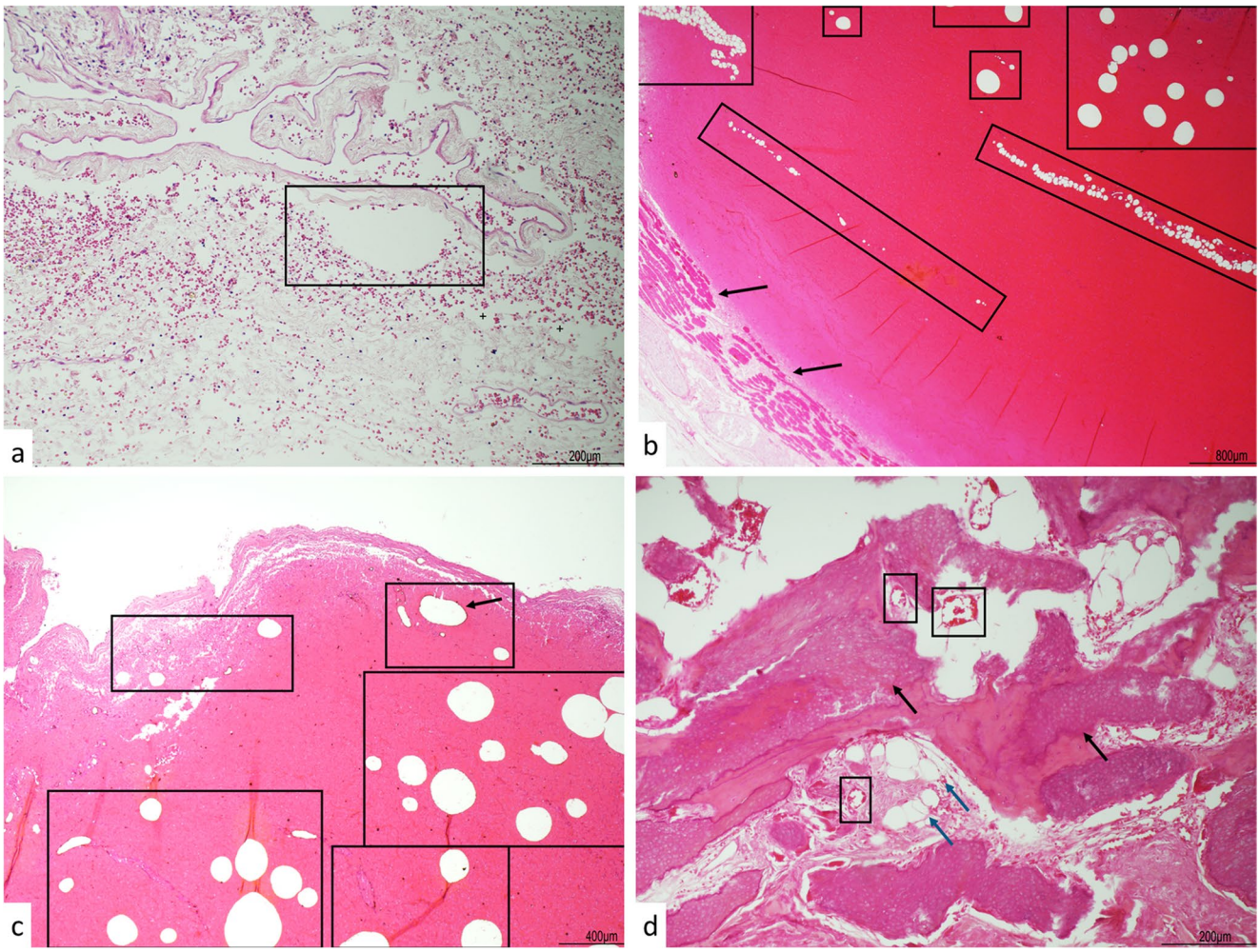

Fig. 2 Central nervous system and cranial soft tissues. (**a**) Subarachnoid space, hemorrhage (10×): Extravascular OES (black box) within subarachnoid hemorrhage. (**b**) Galea, hemorrhage (2×): Extravascular OES (black boxes) within hemorrhagic infiltration. Preservation of the overlying skin structures (black arrows), without postmortem degenerative changes, supports the artifactual nature of OES and helps exclude putrefaction-related gas bubbles. (**c**) Galea and periosteum, hemorrhage (5×): OES (black boxes) within hemorrhagic infiltration, frequently bordered by peripheral dark granular material (black arrow). (**d**) Galeal osteoma (10×): Bone trabeculae (black arrows) and adjacent adipose tissue (blue arrows) are observed. OES (black boxes) are present within vascular spaces. Adipocytes (blue arrows) are distinguishable from OES by their extravascular localization, well-defined cytoplasmic membranes, and characteristic vacuolar morphology

structures were distinguishable from OES because of their irregular shape and extraluminal localization (Fig. 3c).

In lung samples with *chronic sclerosing interstitial lung disease* showing a UIP pattern, intravascular OES and vascular hyperemia were observed (Fig. 4a).

In *mediastinal hemorrhages*, OES were identified both within vascular lumina (intravascular OES) and within hemorrhagic infiltrates (extravascular OES) (Fig. 4b).

Genitourinary and female reproductive system

The pathological findings identified in the genitourinary and female reproductive system included hemorrhagic lesions of the bladder and an ovarian cystic lesion.

The *hemorrhagic bladder lesions* were incidentally observed in the peripheral portion of a histological section primarily sampled from the prostate gland. In these areas, intravascular OES and vascular dilatation were observed. Extravascular OES were also present within intramucosal hemorrhages (Fig. 5).

An *ovarian cystic lesion* was also identified; however, no significant MPMCTA-related histological artifacts were observed in the ovarian tissue.

Liver and pancreas

The pathological processes identified in these organs included hepatic steatosis, metastatic pancreatic adenocarcinoma, and pancreatic neoplastic necrosis.

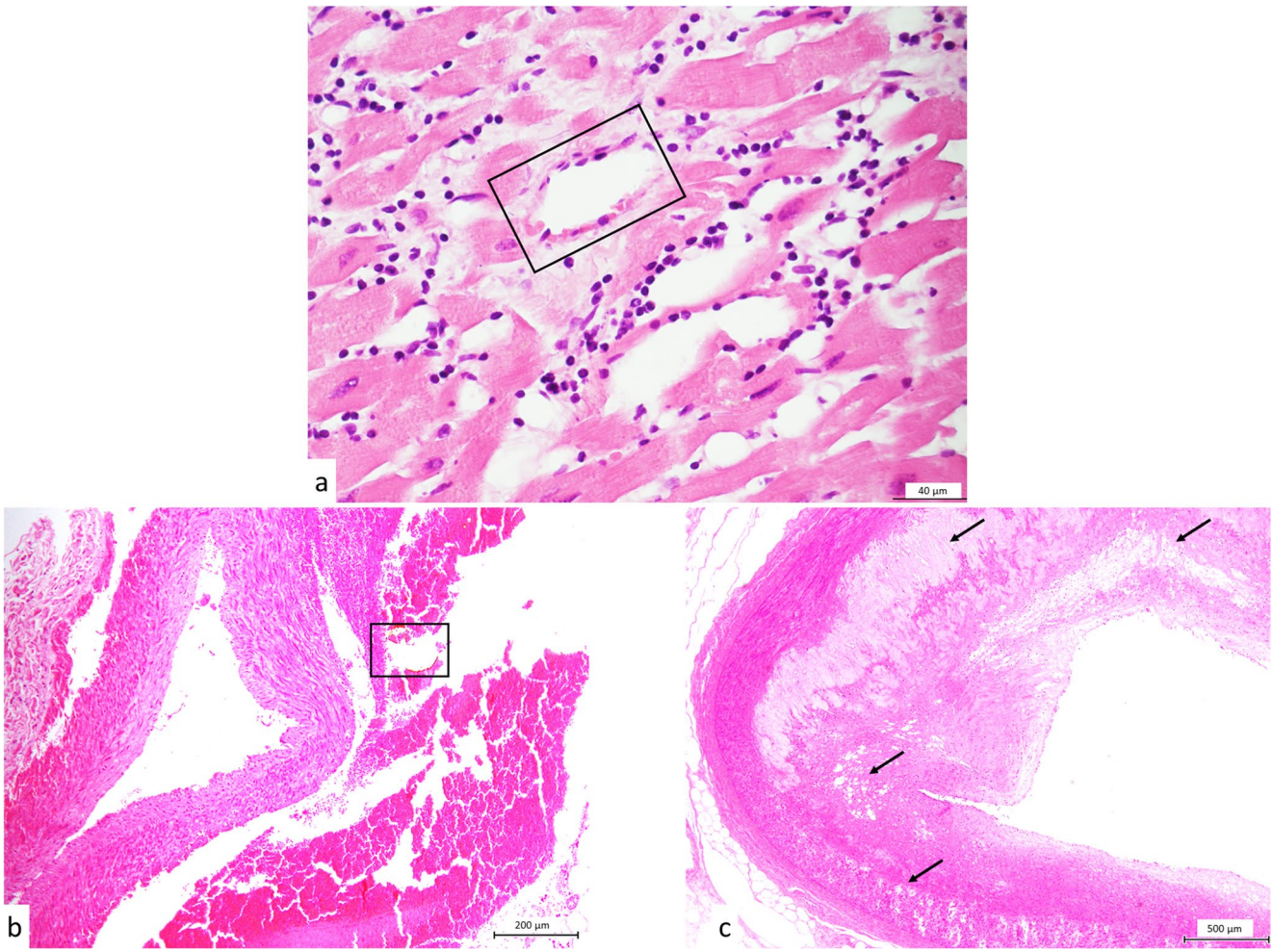

Fig. 3 Cardiovascular system. (**a**) Left ventricular wall, myocarditis (40×): Diffuse lymphocytic infiltration surrounding myocardial fibers, consistent with inflammatory involvement. An intravascular OES (black box) is present. (**b**) Coronary artery dissection (10×): OES (black box) within periluminal hemorrhagic infiltration. (**c**) Coronary artery, fibro-lipidic atherosclerotic plaque (4×): Numerous cholesterol clefts (black arrows), characterized by elongated and irregular empty spaces within the plaque. These are distinguishable from OES by their extraluminal localization and irregular morphology, whereas OES typically show more regular contours and intravascular distribution

In *hepatic steatosis* samples, steatotic hepatocytes were recognizable by cytoplasmic lipid vacuoles and displaced nuclei. OES were observed within sinusoidal capillaries, often compressing erythrocytes; vascular dilatation was also observed (Fig. 6a–c).

In cases of *pancreatic adenocarcinoma metastasis to the liver*, large necrotic areas were identified, in which no contrast-related artifact was found (Fig. 7a).

In pancreatic samples showing *neoplastic necrosis*, intravascular and extravascular OES were observed, often displaying a heterogeneous distribution (Fig. 7b and c).

The principal findings are summarized in Table 1.

Discussion

The present study extends our previous investigation on histo-morphological artifacts induced by multiphase postmortem computed tomography angiography (MPMCTA) by focusing on their appearance in pathological tissues.

While prior studies have described contrast-related artifacts in normal tissues [10], and recent reviews have highlighted the expanding role of postmortem imaging in forensic practice [13], our findings demonstrate that the same principal categories—OES, vascular dilatation, vascular hyperemia, and compression of adjacent structures—are consistently observed in pathological specimens.

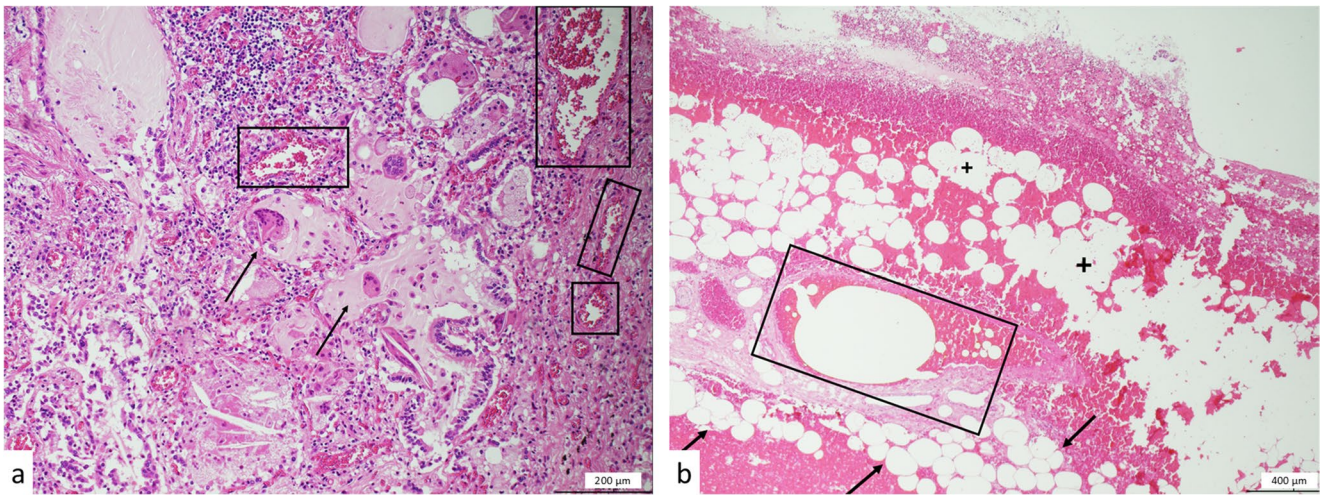

Fig. 4 Thoracic structures. (**a**) Lung, chronic sclerosing interstitial lung disease (10×): Usual interstitial pneumonia (UIP) pattern with fibrotic remodeling of the parenchyma. Intra-alveolar cholesterol clefts (black arrows), surrounded by multinucleated giant cells, are observed. Intravascular OES (black boxes) are present, representing contrast medium within vascular lumina. Vascular hyperemia was also found. (**b**) Mediastinal hemorrhage (5×): Adipocytes (black arrows) and OES within vascular lumina (black box) and hemorrhagic infiltration (black plus signs) are observed. OES can be distinguished from adipocytes by the absence of cytoplasmic membranes and their intravascular or irregular extravascular distribution within hemorrhagic areas

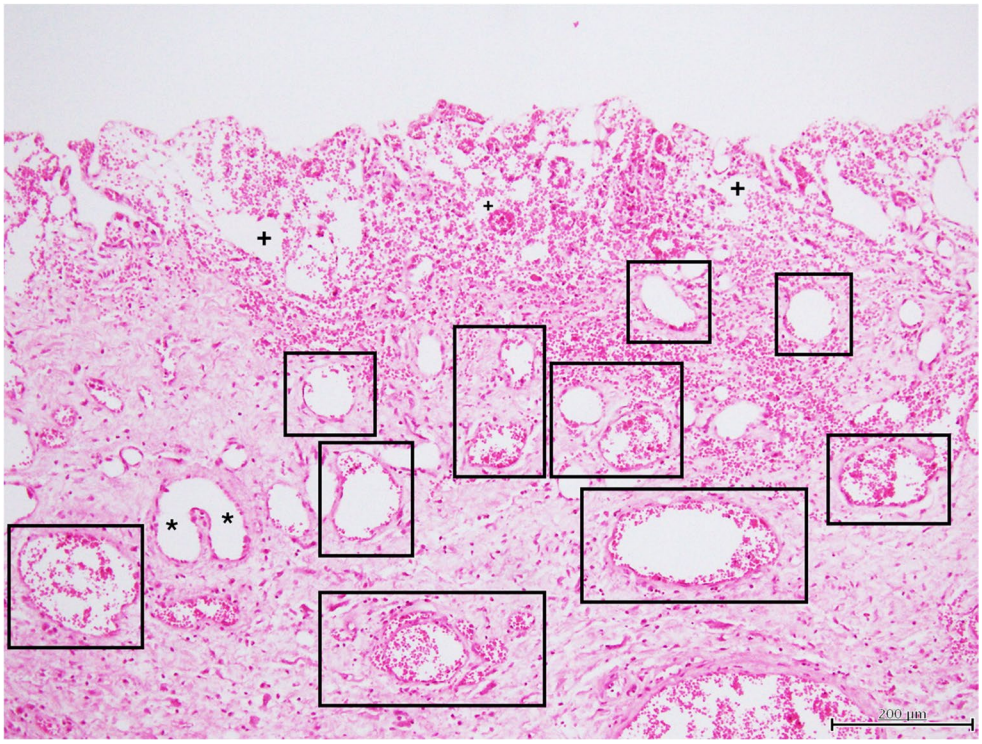

Fig. 5 Genitourinary system. Bladder, hemorrhage (10×): Intravascular OES (black boxes) associated with vascular dilatation (black asterisks), as well as extravascular OES within intramucosal hemorrhage (black plus signs), reflecting both vascular filling and leakage of contrast medium into surrounding tissue

The findings observed in pathological tissues suggest that pre-existing alterations of vascular integrity and tissue architecture may significantly influence the morphology and distribution of MPMCTA-related histological artifacts. Inflammatory vascular damage, hemorrhagic infiltration, necrosis, fibrosis, and tissue disruption may alter both contrast medium diffusion and intravascular retention, leading to heterogeneous perfusion patterns and facilitating the appearance of extravascular OES within structurally altered tissues.

In contrast to the relatively homogeneous artifact distribution previously observed in normal tissues, pathological conditions frequently showed irregular localization of OES and variable degrees of vascular dilatation and hyperemia. These findings suggest the hypothesis that underlying pathological substrates may directly modify the

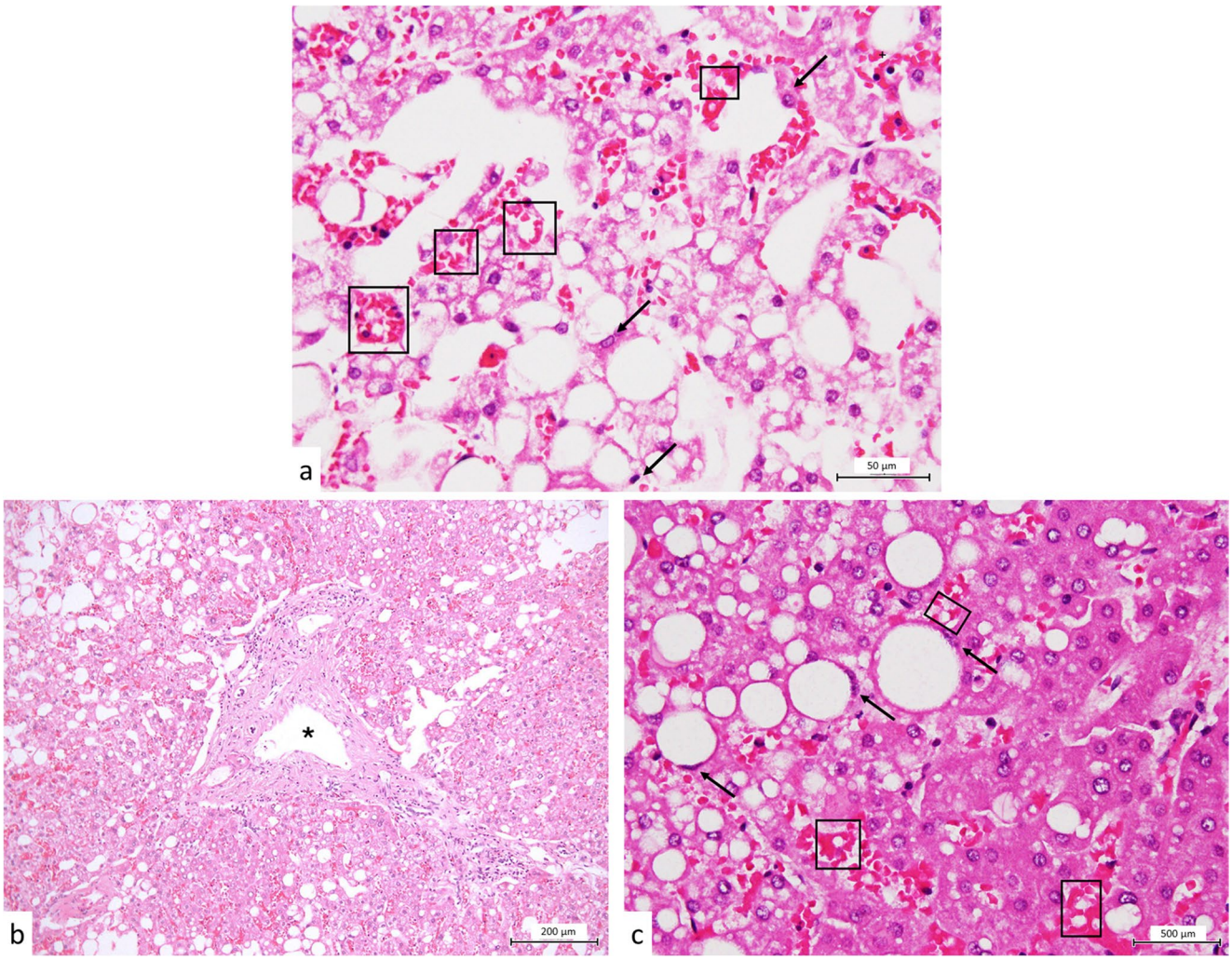

Fig. 6 Liver, hepatic steatosis. (**a**) Liver (20×): Hepatic steatosis with hepatocytes containing lipid vacuoles and displaced nuclei (black arrows). OES (black boxes) within sinusoidal capillaries compress adjacent erythrocytes, consistent with intravascular localization of contrast medium. (**b**) Liver (10×): Diffuse steatosis with dilated centrolobular veins (black asterisks), reflecting vascular distension induced by contrast perfusion. (**c**) Liver (40×): Lipid vacuoles (black arrows) and OES (black box) within sinusoids are observed. OES compress erythrocytes and lack cellular boundaries, allowing differentiation from lipid vacuoles, which are extravascular and defined by cytoplasmic membranes and nuclei

histomorphological appearance of contrast-related artifacts following MPMCTA.The development of these artifacts is closely related to the mechanism of postmortem angiographic perfusion. The injection of an oily contrast agent under controlled pressure leads to displacement of blood and distension of the vascular system, resulting in non-physiological vascular filling patterns [5, 6, 8]. The physical properties of the contrast medium, particularly its viscosity, together with injection pressure, play a crucial role in determining vascular filling and the resulting histo-morphological alterations [6]. These mechanisms account for the formation of OES, vascular dilatation, hyperemia, and compression of adjacent structures, which represent the principal artifact categories observed after MPMCTA [8]. While these processes are well established in normal tissues, their interaction with altered tissue architecture in pathological conditions remains incompletely characterized.

In our series, OES were observed both within vascular lumina and in extravascular compartments, particularly in hemorrhagic and necrotic areas. This dual distribution reflects two complementary mechanisms: intravascular retention of contrast medium within distended vessels and extravascular diffusion or redistribution in structurally compromised tissues. Hemorrhagic lesions, such as subarachnoid and galeal hemorrhages, showed OES embedded within blood infiltrates, supporting passive leakage of contrast medium into extravascular spaces. Similarly, in necrotic neoplastic areas, OES displayed a markedly heterogeneous distribution, with alternating regions of accumulation and absence, likely reflecting uneven perfusion related to disrupted vascular

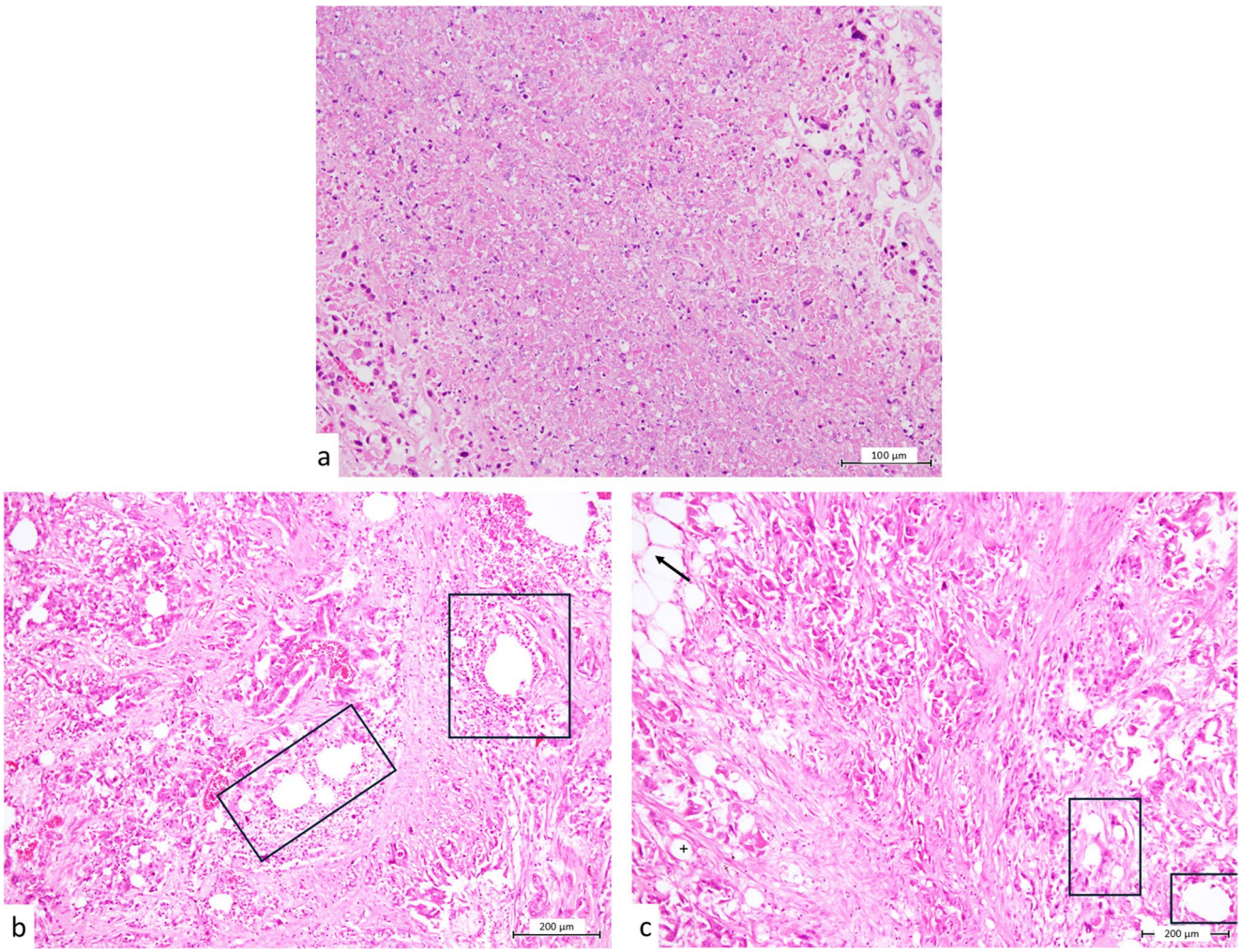

Fig. 7 Liver and pancreas, neoplastic conditions. (**a**) Liver, metastasis of pancreatic adenocarcinoma (20×): Metastatic neoplastic proliferation with extensive necrotic areas, without evidence of contrast medium–related artifacts, indicating absence of contrast penetration in necrotic tissue (**b**) Pancreas, adenocarcinoma (10×): Extravascular OES (black boxes) within neoplastic necrosis, showing heterogeneous distribution of contrast medium (**c**) Pancreas, adenocarcinoma (10×): Adipose tissue (black arrow) adjacent to neoplastic necrosis with intravascular OES (black plus signs). OES can be distinguished from adipocytes by the absence of cytoplasmic membranes and by their irregular distribution within necrotic tissue. Extravascular OES (black boxes) can also be appreciated

supply. These findings are consistent with previous observations of irregular or incomplete perfusion in pathological tissues during postmortem angiography [14].

In the central nervous system, the distinction between true pathological structures and artifacts was generally preserved. Corpora amylacea, as observed in cerebellar cortical atrophy, were readily identifiable due to their extravascular localization and well-defined morphology, which excludes an artifactual origin. However, in cortical samples, the coexistence of vascular dilatation and perivascular lymphocytic infiltration may closely mimic inflammatory vascular conditions. In this context, the absence of vessel wall damage or necrosis represents a key criterion for excluding true vasculitis, highlighting a relevant diagnostic pitfall in the interpretation of postmortem specimens after MPMCTA.

In cardiovascular pathology, inflammatory conditions such as myocarditis demonstrated the coexistence of lymphocytic infiltration with intravascular OES, likely reflecting increased vascular permeability and contrast retention. In coronary artery dissection, OES associated with dark granular residues were observed within hemorrhagic planes, indicating contrast distribution along dissected vascular structures. In contrast, in atherosclerotic plaques, cholesterol clefts were reliably distinguishable from OES based on their irregular morphology and extraluminal localization, whereas OES typically showed more regular contours and intravascular distribution.

In thoracic and soft tissue lesions, OES were frequently identified within both vascular lumina and hemorrhagic infiltrates. In lung tissue with a usual interstitial pneumonia

Table 1 Pathological conditions analyzed in the study and principal observed MPMCTA-related histological artifacts

Organ/Tissue	Number of pathological samples analyzed	Pathological conditions observed	Principal contrast-related artifacts observed
Central nervous system and adjacent cranial tissues	Cortex ($n=7$); Cerebellum ($n=2$)	Cortical atrophy; meningioma; perivascular lymphocytic infiltration; subarachnoid hemorrhage; galeal hemorrhage; galeal osteoma	Intravascular and extravascular OES; vascular dilatation
Cardiovascular system	Heart ($n=54$); Vessels ($n=97$)	Myocarditis; coronary artery dissection; fibro-lipidic atherosclerotic plaques	Intravascular and extravascular OES; compression artifacts
Respiratory system	Lung ($n=18$)	Chronic sclerosing interstitial lung disease (UIP pattern); mediastinal hemorrhage	Intravascular and extravascular OES; vascular hyperemia
Genitourinary and female reproductive system	Ovary ($n=1$); Prostate section with incidental bladder involvement	Ovarian cystic lesion; Hemorrhagic lesions of the bladder	Intravascular and extravascular OES; vascular dilatation
Liver	Liver ($n=9$)	Hepatic steatosis; metastatic pancreatic adenocarcinoma	Sinusoidal dilatation; intravascular OES
Pancreas	Pancreas ($n=2$)	Pancreatic neoplastic necrosis	Intravascular and extravascular OES

pattern, intravascular OES coexisted with intra-alveolar cholesterol clefts, which could be distinguished by their morphology and histiocytic reaction. In mediastinal hemorrhage, the differentiation between OES and adipocytes represents another relevant diagnostic challenge. Adipocytes are characterized by extravascular localization and well-defined cytoplasmic membranes, whereas OES lack cellular boundaries and may appear within vascular or hemorrhagic compartments.

Degenerative conditions such as hepatic steatosis provide a paradigmatic example of artifact–pathology interaction. In these cases, OES were observed within sinusoidal capillaries, often compressing adjacent erythrocytes, confirming their intravascular localization. In contrast, lipid vacuoles within hepatocytes are extravascular and characterized by cytoplasmic membranes and displaced nuclei, allowing reliable differentiation. Additionally, vascular dilatation and sinusoidal distension were frequently observed, reflecting the hemodynamic effects of contrast perfusion.

In neoplastic conditions, including meningiomas and metastatic pancreatic adenocarcinoma, the underlying tumor architecture remained identifiable despite the presence of widespread artifacts. In meningiomas, OES and vascular dilatation were superimposed on preserved neoplastic structures, indicating that contrast-related changes do not obscure fundamental histological features. Conversely, in metastatic and pancreatic tumors, necrotic areas exhibited highly heterogeneous contrast distribution, suggesting limited or uneven penetration of the contrast medium into necrotic tissue.

The coexistence of pathological alterations and contrast-related artifacts introduces several diagnostic pitfalls [15, 16]. OES may mimic fat embolism, gas embolism, or cholesterol clefts, while vascular dilatation and hyperemia may resemble inflammatory vascular processes. In particular, in hemorrhagic and decompositional contexts, empty spaces must be interpreted cautiously, as putrefaction-related gas bubbles may produce similar appearances. The distinction relies on tissue preservation, anatomical localization, and the presence of contrast-related residues. The oily nature of the contrast agent may also simulate fat embolism, especially in pulmonary tissue, as previously reported [9].

The differentiation between contrast-related artifacts and gas-related findings may represent an additional diagnostic challenge. Postmortem gas may result from decomposition processes and typically shows characteristic distribution patterns that differ from pathological gas collections, although overlap may occur. Careful evaluation of gas distribution, volume, and associated findings, as well as correlation with postmortem interval and clinical context, are essential for correct interpretation [17, 18].

Recognition of contrast-related artifacts relies on a combination of morphological criteria and anatomical context. OES typically present with round or semilunar contours, are frequently associated with dark granular residues, and are predominantly intravascular, although extravascular distribution may occur in damaged tissues. In contrast, adipocytes and lipid vacuoles are delimited by cytoplasmic membranes and show characteristic tissue localization, while cholesterol clefts exhibit irregular morphology and specific distribution patterns. Correlation with the overall histological context and, when available, radiological findings remain essential for accurate interpretation.

Despite these challenges, the recognition of the underlying pathological process was generally preserved in our series. Inflammatory conditions, neoplastic architectures, and degenerative changes remained identifiable even in the presence of OES and vascular alterations, confirming that contrast-induced artifacts do not preclude histopathological diagnosis when appropriately recognized [19].

An additional relevant finding is the heterogeneous distribution of contrast-related artifacts in pathological tissues, in contrast to the more uniform patterns observed in normal organs. This variability likely reflects alterations in vascular integrity and tissue architecture and may have practical implications for targeted tissue sampling during autopsy, particularly in heterogeneous lesions.

From a forensic perspective, these findings highlight the importance of integrating radiological, macroscopic, and histological data in postmortem investigations. While MPMCTA represents a valuable tool for detecting vascular lesions [1, 2, 4], its potential to introduce histological artifacts must be carefully considered. The integration of imaging, autopsy, and histology has been increasingly applied in forensic practice, emphasizing the need for multidisciplinary interpretation [20–24]. Failure to recognize these artifacts may lead to misinterpretation and, in some cases, incorrect conclusions regarding the cause of death [25, 26].

Interpretation of postmortem gas findings should always consider the distribution, volume, and anatomical localization of gas, together with the overall radiological and pathological context. Previous studies by Egger et al. [26, 27] demonstrated that postmortem gas follows relatively reproducible distribution patterns during cadaveric alteration and proposed the Radiological Alteration Index (RA-Index) as a standardized tool for assessing decomposition-related radiological changes. These observations are particularly relevant in the context of MPMCTA interpretation, since decomposition-related vascular and parenchymal alterations may further complicate the differentiation between procedure-related artifacts and true pathological findings. As previously observed in postmortem MDCT studies, postmortem gas formation and distribution are influenced by multiple factors beyond the postmortem interval itself, including tissue conditions, vascular integrity, and decomposition-related changes. These mechanisms may also contribute to heterogeneous contrast distribution and artifact formation following MPMCTA in pathological tissues.

The present study has a descriptive and exploratory design and was conceived as a complementary extension of our previous investigation on normal tissues, performed using the same MPMCTA protocol, histological workflow, and interpretative criteria. Unlike controlled experimental studies, the present work reflects routine forensic practice, in which pathological tissues are frequently encountered during postmortem histopathological evaluation. Within this context, the primary objective was not to establish quantitative comparisons between pathological and non-pathological tissues, but rather to systematically characterize the morphology and distribution of contrast-related histological artifacts in the presence of underlying pathological alterations. A formal inter- or intra-observer agreement analysis was not performed because of the exploratory and descriptive design of the study. Nevertheless, histological findings were evaluated by experienced forensic pathologists and consensus review was performed in cases of interpretative uncertainty.

Although postmortem interval (PMI) may potentially influence vascular integrity, tissue preservation, and contrast medium distribution, the present study was not specifically designed to investigate correlations between PMI and the prevalence or severity of MPMCTA-related histological artifacts. Nevertheless, none of the included cases showed advanced putrefactive changes. Further studies involving larger and more homogeneous cohorts are needed to better clarify the possible relationship between PMI and artifact formation.

This study has several limitations, including its single-center retrospective design, the heterogeneity of pathological conditions, and the lack of quantitative assessment of artifact distribution and severity. The retrospective nature of the study and the selection of forensic autopsy cases may represent potential sources of selection bias and may limit the generalizability of the findings. Nevertheless, the analyzed cohort reflects routine medico-legal practice and allowed the evaluation of a broad spectrum of pathological conditions potentially associated with altered contrast distribution and artifact formation following MPMCTA.

In conclusion, MPMCTA is associated with reproducible histomorphological alterations that may also involve pathological tissues. The morphology and distribution of these artifacts appear to be influenced by the underlying pathological substrate and may occasionally generate complex differential diagnostic scenarios during forensic histopathological evaluation. Although contrast-related artifacts may complicate microscopic interpretation, careful correlation between histological findings, tissue architecture, and radiological context generally allows recognition of the underlying pathological process. The present findings should therefore be interpreted within the exploratory and descriptive nature of the study and may contribute to improving awareness of MPMCTA-related artifacts in routine forensic practice.

Author contributions J.C.: writing—original draft, review and editing; microscopy and image production. G.B.G., M.P.B., A.L.S.: microscopy and image production. M.P.B., R.C., E.S., A.L.S.: writing—review and editing. G.B., L.A., P.G., P.T.: radiological data curation. All authors have read and agreed to the published version of the manuscript.

Funding Open access funding provided by Università degli Studi di Parma within the CRUI-CARE Agreement. No funds, grants, or other support was received.

Data availability All relevant data are included in the manuscript.

Declarations

Ethics approval not applicable.

Consent not applicable.

Competing interests The authors declare that they have no known competing financial interests or personal relationships that could have appeared to influence the work reported in this paper.

References

1. Michaud K, Grabherr S, Jackowski C, Bollmann MD, Doenz F, Mangin P. Postmortem imaging of sudden cardiac death. Int J Legal Med. 2014;128:127–37. https://doi.org/10.1007/s00414-013-0819-6.
2. Michaud K, Jacobsen C, Basso C, Banner J, Blokker BM, de Boer HH, et al. Application of postmortem imaging modalities in cases of sudden death due to cardiovascular diseases: current achievements and limitations from a pathology perspective. Virchows Arch. 2023;482:385–406. https://doi.org/10.1007/s00428-022-03458-6.
3. Dedouit F, Ducloyer M, Elifritz J, Adolphi NL, Yi-Li GW, Decker S, et al. The current state of forensic imaging: post-mortem imaging. Int J Legal Med. 2025;139:1141–59. https://doi.org/10.1007/s00414-025-03461-x.
4. Norberti N, Tonelli P, Giaconi C, Nardi C, Focardi M, Nesi G, et al. State of the art in post-mortem computed tomography: a review of current literature. Virchows Arch. 2019;475:139–50. https://doi.org/10.1007/s00428-019-02562-4.
5. Grabherr S, Rinaldi A, Dominguez A, Pomara C. Multiphase postmortem computed tomography angiography (MPMCTA). In: Grabherr S, Grimm JM, Heinemann A, editors. Atlas of postmortem angiography. Springer; 2016.
6. Stumm CJ, Wittig H, Kalberer NM, Scheurer E. Histomorphological assessment of isolated abdominal organs after targeted perfusion with the contrast agent Angiofil® in postmortem computed tomography angiography. Forensic Sci Int. 2020;315:110427. https://doi.org/10.1016/j.forsciint.2020.110427.
7. Jessika C, Anna Laura S, Stefano D, Giuliano Bruno G, Marco B, Riccardo B, Riccardo R, Enrico S. Diagnosing coronary thrombosis using multiphase post-mortem CT angiography (MPMCTA): a case study. Med Sci Law. 2021;61:77–81. https://doi.org/10.1177/0025802420923175.
8. Wittig H, Stumm C, Eplinius F, Hecht L. Histology after postmortem angiography. In: Grabherr S, Grimm JM, Heinemann A, editors. Atlas of postmortem angiography. Springer; 2016.
9. Capuani C, Guilbeau-Frugier C, Mokrane FZ, Delisle MB, Marcheix B, Rousseau H, Telmon N, Rougé D, Dedouit F. Tissue microscopic changes and artifacts in multi-phase post-mortem computed tomography angiography in a hospital setting: a fatal case of systemic vasculitis. Forensic Sci Int. 2014;242:e12–7. https://doi.org/10.1016/j.forsciint.2014.06.039.
10. Camatti J, Gangi BG, Bonasoni MP, Battinelli G, Alemanno L, Pizzuti G, Torricelli P, Silingardi E, Cecchi R, Santunione AL. Histological artifacts induced by the contrast agent in multi-phase post-mortem CT angiography (MPMCTA): Part I – normal tissues. Forensic Sci Med Pathol. 2025. https://doi.org/10.1007/s12024-025-01117-1.
11. TWGPAM. Title of subordinate document. In: TWGPAM presentation. https://www.twgpam.org/twgpam-presentation/. Accessed 17 Mar 2026.
12. Brinkmann B. Harmonization of medico-legal autopsy rules. Int J Legal Med. 1999;113:1–14. https://doi.org/10.1007/s004140050271.
13. Dedouit F, Ducloyer M, Elifritz J, Adolphi NL, Yi-Li GW, Decker S, Ford J, Kolev Y, Thali M. The current state of forensic imaging: perspectives. Int J Legal Med. 2025;139:2819–27. https://doi.org/10.1007/s00414-025-03466-6.
14. O'Donnell C, Hislop-Jambrich J, Woodford N, Baker M. Demonstration of liver metastases on postmortem whole body CT angiography following inadvertent systemic venous infusion of the contrast medium. Int J Legal Med. 2012;126:311–4. https://doi.org/10.1007/s00414-012-0669-7.
15. Bruguier C, Mosimann PJ, Vaucher P, Uské A, Doenz F, Jackowski C, et al. Multi-phase postmortem CT angiography: recognizing technique-related artefacts and pitfalls. Int J Legal Med. 2013;127:639–52. https://doi.org/10.1007/s00414-013-0840-9.
16. Bruch GM, Grabherr S, Bruguier C, Fischer FT, Soto R, Magnin V, et al. Development of a protocol for standardized use of a water-soluble contrast agent with polyethylene glycol in postmortem CT angiography. Int J Legal Med. 2024;138:1437–46. https://doi.org/10.1007/s00414-024-03218-y.
17. Wong YL, Hamdan AN, Chainchel Singh MK, Siew SF. Postmortem computed tomography differentiation of putrefactive gas and air embolism. Malays J Pathol. 2023;45:139–43.
18. Hussein MN, Heinemann A, Shokry DA, Elgebely M, Pueschel K, Hassan FM. Postmortem computed tomography differentiation between intraperitoneal decomposition gas and pneumoperitoneum. Int J Legal Med. 2022;136:229–35. https://doi.org/10.1007/s00414-021-02732-7.
19. Higgins S, Parsons S, Woodford N, Lynch M, Briggs C, O'Donnell C. The effect of post-mortem computed tomography angiography on histological analysis. Forensic Sci Med Pathol. 2017;13:317–27. https://doi.org/10.1007/s12024-017-9871-8.
20. Camatti J, Santunione AL, Draisci S, Antonella D, Amorico MG, Ligabue G, et al. Predictive value of coronary artery calcium score on radiological and autoptic findings in cases of sudden death. Forensic Imaging. 2024;39:200610. https://doi.org/10.1016/j.fri.2024.200610.
21. Camatti J, Santunione AL, Draisci S, Antonella D, Amorico MG, Ligabue G, et al. Correlation between epicardial fat volume and postmortem findings. Forensic Imaging. 2025;40:200620. https://doi.org/10.1016/j.fri.2024.200620.
22. Santunione AL, Camatti J, Battinelli G, Alemanno L, Pizzuti G, Torricelli P, et al. Application of multiphase post-mortem CT angiography in hemoptysis. Forensic Imaging. 2025;43:200653. https://doi.org/10.1016/j.fri.2025.200653.
23. Sabatasso S, Vanhaebost J, Doenz F, Palmiere C, Michaud K, Dedouit F, et al. Visualization of myocardial infarction in postmortem MPMCTA. Am J Forensic Med Pathol. 2018;39:106–13. https://doi.org/10.1097/PAF.0000000000000372.
24. Morgan B, Biggs MJ, Barber J, Raj V, Amoroso J, Hollingbury FE, et al. Accuracy of post-mortem CT coronary angiography. Int J Legal Med. 2013;127:809–17. https://doi.org/10.1007/s00414-012-0790-7.

25. Berger N, Martinez R, Winklhofer S, Flach PM, Ross S, Ampanozi G, et al. Pitfalls in post-mortem CT angiography. Leg Med (Tokyo). 2013;15:315–7. https://doi.org/10.1016/j.legalmed.2013.07.001.
26. Wiskott K, Magnin V, Egger C, Soto R, Grabherr S, Fracasso T. Diagnostic tips for multiphase post-mortem CT angiography. Int J Legal Med. 2026;140:291–300. https://doi.org/10.1007/s00414-025-03593-0.
27. Egger C, Bize P, Vaucher P, Mosimann P, Schneider B, Dominguez A, et al. Distribution of artifactual gas on post-mortem multidetector computed tomography (MDCT). Int J Legal Med. 2012;126(1):3–12. https://doi.org/10.1007/s00414-010-0542-5.
28. Egger C, Vaucher P, Doenz F, Palmiere C, Mangin P, Grabherr S. Development and validation of a postmortem radiological alteration index: the RA-Index. Int J Legal Med. 2012;126(4):559–66. https://doi.org/10.1007/s00414-012-0686-6.

Authors and Affiliations

Jessika Camatti[1] · Bruno Giuliano Gangi[2] · Maria Paola Bonasoni[3] · Giovanni Battinelli[4] · Luca Alemanno[4] · Giovanni Pizzuti[4] · Pietro Torricelli[5] · Enrico Silingardi[5] · Rossana Cecchi[5] · Anna Laura Santunione[5]

✉ Jessika Camatti
jessika.camatti@unipr.it

Bruno Giuliano Gangi
b.gangi@ausl.mo.it

Maria Paola Bonasoni
MariaPaola.Bonasoni@ausl.re.it

Giovanni Battinelli
battinelli.giovanni@aou.mo.it

Luca Alemanno
alemanno.luca@aou.mo.it

Giovanni Pizzuti
pizzuti.giovanni@aou.mo.it

Pietro Torricelli
pietro.torricelli@unimore.it

Enrico Silingardi
enrico.silingardi@unimore.it

Rossana Cecchi
rossana.cecchi@unimore.it

Anna Laura Santunione
annalaura.santunione@unimore.it

[1] University of Parma, Parma, Italy

[2] AUSL Modena, Modena, Italy

[3] AUSL Reggio Emilia, Reggio Emilia, Italy

[4] University Hospital Modena, Modena, Italy

[5] University of Modena and Reggio Emilia, Modena, Italy